Steel and Composite Structures, *Vol. 35, No. 1* (*2020*) *61-76*
DOI: https://doi.org/10.12989/scs.2020.35.1.061

An inclined FGM beam under a moving mass considering Coriolis and centrifugal accelerations

Vahid Shokouhifard[1], Saeedreza Mohebpour*[1,2], Parviz Malekzadeh[1] and Hekmat Alighanbari[2]

[1]*Department of Mechanical Engineering, Persian Gulf University, Bushehr, 7516913798, Iran*
[2]*Department of Aerospace Engineering, Ryerson University, Toronto, ON, M5B 2K3, Canada*

(*Received July 30, 2019, Revised February 28, 2020, Accepted March 5, 2020*)

Abstract. In this paper, the dynamic behaviour of an inclined functionally graded material (FGM) beam with different boundary conditions under a moving mass is investigated based on the first-order shear deformation theory (FSDT). The material properties vary continuously along the beam thickness based on the power-law distribution. The system of motion equations is derived by using Hamilton's principle. The finite element method (FEM) is adopted to develop a general solution procedure. The moving mass is considered on the top surface of the beam instead of supposing it on the mid-plane. In order to consider the Coriolis, centrifugal accelerations and the friction force, the contact force method is used. Moreover, the effects of boundary conditions, the moving mass velocity and various material distributions are studied. For verification of the present results, a comparative fundamental frequency analysis of an FGM beam is conducted and the dynamic transverse displacements of the homogeneous and FGM beams traversed by a moving mass are compared with those in the existing literature. There is a good accord in all compared cases. In this study for the first time in dynamic analysis of the inclined FGM beams, the Coriolis and centrifugal accelerations of the moving mass are taken into account, and it is observed that these accelerations can be ignored for the low-speeds of the moving mass. The new provided results for dynamics of the inclined FGM beams traversed by a moving mass can be significant for the scientific and engineering community in the area of FGM structures.

Keywords: inclined Timoshenko beam; FGM; moving mass; Coriolis; centrifugal; friction; FEM

1. Introduction

The problem of a beam under moving masses has been of interest for several decades. A wide range of analytical and numerical methods have been developed along the time to investigate the dynamic behaviour of all customary and non-customary components and structures using isotropic, composite and FGM models. Jeffcott introduced this at first in 1929 and was closely followed by Steuding and Odman (Stanišić and Hardin 1969). Their solutions to the problem were presented in an approximate form involving rather laborious permutation techniques. Investigations regarding the problem of moving load are considerable, e.g., Xu *et al.* (1997) applied the finite difference method and the perturbation technique to study the longitudinal and transverse motions of a finite elastic beam subjected to a moving mass. Michaltsos *et al.* (1996) inquired into the mass and velocity influence of the moving load on the linear dynamic response of a simply-supported uniform beam. Dyniewicz *et al.* (2019) investigated the dynamic behaviour of a nonlinear Gao beam traversed by a moving mass or a massless concentrated force. Shokouhifard *et al.* (2019) presented an inverse dynamic analysis of an inclined FGM beam under a moving load for estimating the mass of moving load based on a conjugate gradient method. Cicirello (2019), Dimitrovová (2019), Froio *et al.* (2018), Greco and Lonetti (2018), Hoang *et al.* (2017), Hou *et al.* (2015), Ichikawa *et al.* (2000), Kadivar and Mohebpour (1998), Kourehli *et al.* (2018), Simsek (2011), Song *et al.* (2017), Stojanović *et al.* (2017), Wu (2004) and Esen and Koç (2015) carried out the dynamic analysis of beams regarding to the moving masses through different analytical or numerical methods. The main studies are limited to the problems that the external load moves on the horizontal beams, while the many contexts of the inclined beams have remained for more investigation.

Also, in the small number of published literature, the effects of Coriolis and centrifugal accelerations of the moving mass are considered in the interaction force between the mass and the beam. The response of a uniform beam excited by a moving mass was determined by Cifuentes (1989), which the introduced technique was based on a Lagrange Multiplier formulation. Wu (2005) studied the dynamic behaviour of an inclined homogeneous beam under a concentrated moving mass, which the moving load on the beam was considered as a moving mass element. Simsek (2010) presented the vibration analysis of a horizontal FGM beam under a moving mass, in which the moving mass was supposed on the mid-plane of the beam. Esen (2011) investigated the dynamic response of a beam due to an accelerating moving mass using moving finite element approximation. Mohebpour *et al.* (2013) studied an inclined flexible beam carrying one degree of freedom moving mass including rotary inertia effects. Mohebpour *et al.* (2016) investigated an inclined cross-ply laminated

*Corresponding author, Associate Professor
E-mail: mohebpour@pgu.ac.ir

ISSN: 1229-9367 (Print), 1598-6233 (Online)

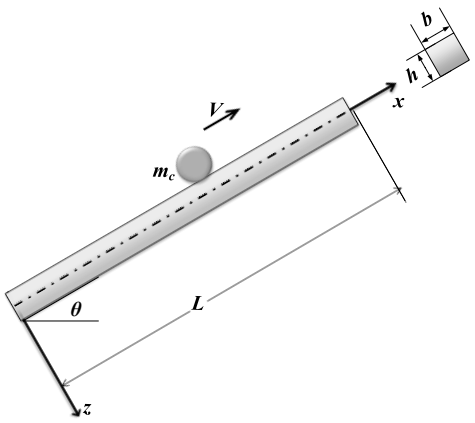

Fig. 1 The inclined FGM beam under a moving concentrated mass m_c

composite beam subjected to a moving mass.

The appearance of FGMs was beginning of a new era in applications of composites in various industries due to their favorable and continuously varying microstructure and mechanical and/or thermal properties (Horii and Nemat-Nasser 1985, Suresh and Mortensen 1998, Thai and Vo 2012, Kim and Reddy 2013, Kocaturk and Akbas 2013, Miyamoto *et al.* 2013, Duy *et al.* 2014, Bourada *et al.* 2015, Chaht *et al.* 2015, Darilmaz 2015, Kar and Panda 2015, Benferhat *et al.* 2016, Burlayenko *et al.* 2017, Chen *et al.* 2017, Arioui *et al.* 2018, Esen *et al.* 2018, Esen 2019, Nguyen and Tran 2018, Cho 2019, Moleiro *et al.* 2019).

This study presents the dynamic behaviour of an inclined FGM beam with different boundary conditions under a moving mass considering the effects of Coriolis, centrifugal accelerations of the moving mass and the friction force between the inclined beam and the moving mass. The moving mass is considered on the top surface of the beam instead of supposing it on the mid-plane of the beam. The new provided results for dynamics of the inclined FGM beams under a moving mass can be noteworthy for the scientific and engineering community in the area of FGM structures.

2. The material gradient of FGM beams

The FGM can be fabricated by continuously varying the constituents of multi-phase materials in a predetermined profile. The preferable features of an FGM member are the inhomogeneous microstructures with continuously graded material properties. An FGM can be defined by the variation of the material properties in terms of the volume fractions. Most researchers use the power-law function (P-FGM) or exponential function (E-FGM) to characterize the volume fractions. However, only there are a few studies that have characterised the volume fractions by using sigmoid function (S-FGM). Therefore, this paper considers an elastic P-FGM beam with rectangular cross-section, in which the material mixture varies along the thickness direction in terms of the volume fraction according to a power-law distribution. As shown in Fig. 1, the spatial coordinate x is defined along the beam length, whereas the z-axis is in the thickness direction, and originated at the middle surface of the beam. The material properties on the upper and lower surfaces of the beam are different but pre-assigned because of compatibility with the performance demands. However, the mass density, the Young's modulus and the Poisson's ratio of the beam vary continuously in the thickness direction (z-axis).

2.1 The material properties of P-FGM beams

It is assumed that the material property gradation is through the thickness, and represented the profile of volume fraction variation by the power-law expression, i.e.

$$P(z) = (P_b - P_t)\Lambda + P_t, \tag{1a}$$

$$\Lambda = (\frac{z}{h} + \frac{1}{2})^k, \tag{1b}$$

where P stand for a generic material property, for instance, the Young's modulus and the mass density, also the property of the top $(z = -h/2)$ and bottom $(z = h/2)$ faces of the beam are denoted by P_t and P_b, respectively, and h is the beam thickness. The material index k would specify the material variation profile through the beam thickness.

3. Theoretical formulations

3.1 General comments

An inclined FGM Timoshenko beam with length L, width b, thickness h and inclination angle θ travelled by a concentrated mass of m_c with constant speed V is considered (see Fig. 1). The rectangular Cartesian coordinate system (x, y, z) is used to indicate the material points of the beam in the unstressed reference configuration. Moreover, it is assumed that the mass is in full contact with the beam, during its motion, i.e. no separation ensues.

3.2 Motion equations of the entire inclined beam itself

It is assumed that the beam deforms in the linear elastic range and hence the generalized Hooke's law is used. In this study, the FSDT is employed to approximate the deformations of the beam and therefore by assuming small deformation, the linear strain-displacement relations are

$$\varepsilon_x = \frac{\partial \bar{u}}{\partial x} = \frac{\partial u}{\partial x} + z\frac{\partial \psi}{\partial x}, \tag{2a}$$

$$\gamma_{xz} = \frac{\partial \bar{u}}{\partial z} + \frac{\partial \bar{w}}{\partial x} = \psi + \frac{\partial w}{\partial x}, \tag{2b}$$

if

$$\bar{u}(x,z,t) = u(x,t) + z\psi(x,t),\ \bar{w}(x,z,t) = w(x,t), \tag{3}$$

in which $\bar{u}(x,z,t)$ is the axial displacement of the beam, $u=u(x,t)$ is the axial displacement of a point on the mid-plane (i.e., $z=0$) of the beam, $w=w(x,t)$ is the transverse displacement of the beam measured downward from its equilibrium configuration, i.e. in the *z*-direction, and $\psi=\psi(x,z,t)$ is the rotation of the beam cross-section due to the beam bending. Furthermore, ε_x and γ_{xz} are the normal strain and transverse shear strain of the beam, respectively. To extract the governing differential equations of motion by employing Hamilton's principle, the kinetic energy (K) and the strain energy (U) of the beam are

$$T=\int_V \frac{\rho}{2}\left[\left(\frac{\partial \bar{u}}{\partial t}\right)^2+\left(\frac{\partial \bar{w}}{\partial t}\right)^2\right]dV, \tag{4}$$

$$U=\frac{1}{2}\int_V (\sigma_x\varepsilon_x+\tau_{xz}\gamma_{xz})dV, \tag{5}$$

where σ_x and τ_{xz} are the axial and transverse shear stresses acting on the beam, respectively. At the boundary points of the beam, the bending moment of a beam section perpendicular to the x-axis, the normal and shear forces are denoted by $\hat{M}_{xx}$, $\hat{N}_{xx}$ and $\hat{Q}_x$, respectively. The work done by the boundary forces and moments is

$$\delta W_{ext}=\left(\hat{N}_{xx}\delta u+\hat{M}_{xx}\delta\psi+\hat{Q}_x\delta w\right)\Big|_0^l. \tag{6}$$

In this study, when the mass enters the left end of the beam, the zero initial conditions are supposed for the beam, i.e. the beam has not any deflection at time $t=0$. The variation of kinetic and strain energy of the FGM beam can be stated as follows.

$$\int_{t_1}^{t_2}\delta T=-\int_{t_1}^{t_2}\int_0^l\left[\left(I_0\frac{\partial^2 u}{\partial t^2}+I_1\frac{\partial^2\psi}{\partial t^2}\right)\delta u+\left(I_1\frac{\partial^2 u}{\partial t^2}+I_2\frac{\partial^2\psi}{\partial t^2}\right)\delta\psi+I_0\frac{\partial^2 w}{\partial t^2}\delta w\right]dxdt, \tag{7}$$

$$\int_{t_1}^{t_2}\delta U dt=\int_{t_1}^{t_2}\int_0^l\left\{\left[\left(A_{11}\frac{\partial u}{\partial x}+B_{11}\frac{\partial\psi}{\partial x}\right)\delta\left(\frac{\partial u}{\partial x}\right)+\left(B_{11}\frac{\partial u}{\partial x}+D_{11}\frac{\partial\psi}{\partial x}\right)\delta\left(\frac{\partial\psi}{\partial x}\right)\right]+k_sA_{55}\left[\left(\psi+\frac{\partial w}{\partial x}\right)\delta\psi+\left(\psi+\frac{\partial w}{\partial x}\right)\delta\left(\frac{\partial w}{\partial x}\right)\right]\right\}dxdt, \tag{8}$$

where

$$[I_0,I_1,I_2,A_{11},B_{11},D_{11},A_{55}]=b\int_{-h/2}^{h/2}[\rho(z),z\rho(z),z^2\rho(z),E(z),zE(z),z^2E(z),G(z)]\mathrm{d}z. \tag{9}$$

It is assumed that Young's modulus (E), shear modulus (G) and mass density (ρ) vary according to Eq. (1a), and the shear correction factor $k_s=5/6$.

By establishing the Lagrangian function of the system as $L=T-(U-W_{ext})$ and applying Hamilton's principle, the variational (or weak) form of the motion equations will be obtained as follows.

$$\int_0^l\left[\left(A_{11}\frac{\partial u}{\partial x}+B_{11}\frac{\partial\psi}{\partial x}\right)\left(\frac{\partial\delta u}{\partial x}\right)+\left(I_0\frac{\partial^2 u}{\partial t^2}+I_1\frac{\partial^2\psi}{\partial t^2}\right)\delta u\right]dx=0, \tag{10a}$$

$$\int_0^l\left[k_sA_{55}\left(\psi+\frac{\partial w}{\partial x}\right)\left(\frac{\partial\delta w}{\partial x}\right)+I_0\frac{\partial^2 w}{\partial t^2}\delta w\right]dx=0, \tag{10b}$$

$$\int_0^l\left[\left(B_{11}\frac{\partial u}{\partial x}+D_{11}\frac{\partial\psi}{\partial x}\right)\left(\frac{\partial\delta\psi}{\partial x}\right)+k_sA_{55}\left(\psi+\frac{\partial w}{\partial x}\right)\delta\psi+\left(I_1\frac{\partial^2 u}{\partial t^2}+I_2\frac{\partial^2\psi}{\partial t^2}\right)\delta\psi\right]dx=0, \tag{10c}$$

and at the boundaries of the beam $(x=0,l)$

$$\begin{cases}\hat{N}_{xx}=0 \text{ or } \delta u=0\\ \hat{Q}_x=0 \text{ or } \delta w=0\\ \hat{M}_{xx}=0 \text{ or } \delta\psi=0\end{cases} \tag{11}$$

3.3 Finite element formulation

Since the primary variables are the dependent unknowns themselves (and do not include their derivative), the dependent variables of the *e*th element of the beam (u^e, w^e and ψ^e) can be approximated by the Lagrange interpolation functions. In this paper, the consistent interpolation procedure is used to overcome the shear locking phenomenon. The nodal displacements of the *e*th element of the beam ($\{u^e\}$, $\{w^e\}$ and $\{\psi^e\}$) are approximated as follows.

$$u^e = \sum_{j=1}^{2} u_j^e \phi_j^{(1)}, \tag{12a}$$

$$w^e = \sum_{j=1}^{3} w_j^e \phi_j^{(2)}, \tag{12b}$$

$$\psi^e = \sum_{j=1}^{2} \psi_j^e \phi_j^{(3)}. \tag{12c}$$

For convenience

$$\left\{u_1^e \quad u_2^e \quad w_1^e \quad w_2^e \quad w_3^e \quad \psi_1^e \quad \psi_2^e\right\}^T =$$

$$\left\{q_1^e \quad q_2^e \quad q_3^e \quad q_4^e \quad q_5^e \quad q_6^e \quad q_7^e\right\}^T = \{q\}^e, \tag{13a}$$

$$\left\{\phi_1^{(1)} \quad \phi_2^{(1)} \quad \phi_1^{(2)} \quad \phi_2^{(2)} \quad \phi_3^{(2)} \quad \phi_1^{(3)} \quad \phi_2^{(3)}\right\}^T =$$

$$\left\{\phi_1 \quad \phi_2 \quad \phi_3 \quad \phi_4 \quad \phi_5 \quad \phi_6 \quad \phi_7\right\}^T. \tag{13b}$$

The applied Lagrange interpolation functions ϕ_k $(k = 1,\ldots,7)$ are defined as follows.

$$\phi_1 = \phi_6 = 1-\varsigma,\ \phi_2 = \phi_7 = \varsigma,\ \phi_3 = 1-3\varsigma+2\varsigma^2,$$
$$\phi_4 = 4\varsigma - 4\varsigma^2,\ \phi_5 = -\varsigma + 2\varsigma^2, \tag{14}$$

where

$$\varsigma = \frac{\bar{x}}{l}. \tag{15}$$

The local *x*-coordinate of any point of the beam element with respect to the left end of the beam element is denoted by $\bar{x}$.

By substituting Eq. (12) into Eq. (10)

$$[M^e]\{\ddot{q}^e\} + [K^e]\{q^e\} = \{Q^e\}, \tag{16}$$

in which $[M^e]$, $[K^e]$, $\{Q^e\}$ and $\{q^e\}$ are the element mass, stiffness matrices, the element nodal force and displacement vectors of the *e*th element of the FGM beam, respectively. The overhead dot indicates the differentiation with respect to time t. The expanded form of $[M^e]$, $[K^e]$ and $\{Q^e\}$ are given in Appendix A. Therefore, the motion equations of the entire FGM beam itself are determined by

$$[M_b]\{\ddot{q}\} + [C_b]\{\dot{q}\} + [K_b]\{q\} = \{Q\}, \tag{17}$$

where $[M_b]$, $[K_b]$, $\{Q\}$ and $\{q\}$ are the overall mass, stiffness matrices, the overall nodal force and displacement vectors of the entire FGM beam itself, respectively, obtained by assembling all its element mass, stiffness matrices and nodal force vectors. The Rayleigh damping theory is applied for extracting the overall damping matrix $[C_b]$ of the FGM beam itself (Bathe 1982).

$$[C_b] = a[M_b] + b[K_b], \tag{18a}$$

$$a = \frac{2\omega_i\omega_j\left(\xi_i\omega_j - \xi_j\omega_i\right)}{\omega_j^2 - \omega_i^2}, \tag{18b}$$

$$b = \frac{2\left(\xi_j\omega_j - \xi_i\omega_i\right)}{\omega_j^2 - \omega_i^2}, \tag{18c}$$

where ξ_i and ξ_j are the damping ratios of the structure corresponding to any two natural frequencies, ω_i and ω_j.

3.4 Force vector and property matrices of the moving mass element

In this study, the effects of Coriolis, centrifugal accelerations of the moving mass and the friction force between the beam and the moving mass are considered. These effects are taken into account by using the contact force method for the beam element that the moving mass is located on it, at any instant of time, and this element is called *moving mass element*.

The local *x*-coordinate of a point of the beam that the moving mass is located on it, which this point of the beam is further named *contact point*, is denoted by $\bar{x}_c$. The moving mass is considered on the top surface of the beam instead of supposing it on the mid-plane of the beam. Therefore, the acceleration component of the contact point in *x*-direction is $\ddot{\bar{u}}_c = \ddot{\bar{u}}(\bar{x}_c, -h/2, t)$. With regarding the centrifugal, Coriolis and inertial accelerations of the moving mass, the interaction forces in *x* and *z* directions ($F_x^{m_c}$ and $F_z^{m_c}$, respectively) are given by using the contact force method as follows.

$$F_x^{m_c} = m_c\left[-\left(\ddot{u}_c - \frac{h}{2}\ddot{\psi}_c\right) - g\sin\theta\right] - \mu F_z^{m_c}, \tag{19a}$$

$$F_z^{m_c} = m_c\left(g\cos\theta - \ddot{w}_c - 2V\dot{w}_c' - V^2 w_c''\right), \tag{19b}$$

where w and ψ for the contact point are denoted by w_c and ψ_c, respectively, and the overhead prime indicates differentiation with respect to coordinate *x*. $F_x^{m_c}$ acts on the upper face of the beam, hence the corresponding moment of it $M_y^{m_c}$ is stated in Eq. (20).

$$M_y^{m_c} = \frac{h}{2} F_x^{m_c}, \tag{20}$$

so

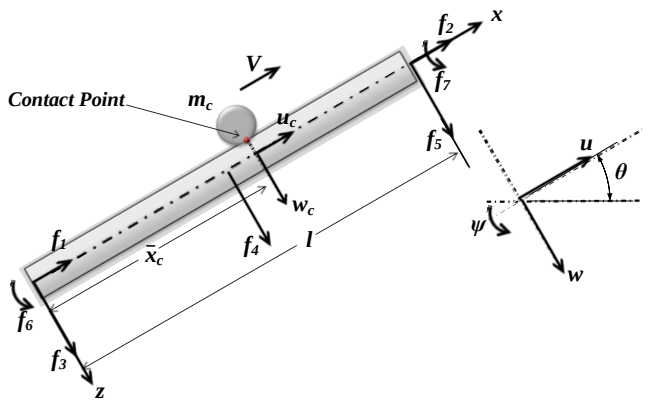

Fig. 2 The equivalent nodal forces (f_1–f_7) of an inclined beam element under a moving concentrated mass m_c

$$M_y^{m_c} = \frac{h}{2} m_c \Bigg[-\left(\ddot{u}_c - \frac{h}{2}\ddot{\psi}_c \right) - g\sin\theta - \mu\big(g\cos\theta - \ddot{w}_c - 2V\dot{w}_c' - V^2 w_c''\big) \Bigg], \tag{21}$$

with

$$\ddot{\bar{u}}_c = \ddot{u}(x_c,t) - \frac{h}{2}\ddot{\psi}(x_c,t) = \ddot{u}_c - \frac{h}{2}\ddot{\psi}_c . \tag{22}$$

Substituting Eqs. (12) and (13) into Eqs. (19) and (21) results in

$$F_x^{m_c} = -m_c[(\phi_1\ddot{q}_1 + \phi_2\ddot{q}_2) - \frac{h}{2}(\phi_6\ddot{q}_6 + \phi_7\ddot{q}_7)] - m_c g\sin\theta - \mu m_c[g\cos\theta - (\phi_3\ddot{q}_3 + \phi_4\ddot{q}_4 + \phi_5\ddot{q}_5) - 2V(\phi_3'\dot{q}_3 + \phi_4'\dot{q}_4 + \phi_5'\dot{q}_5) - V^2(\phi_3''q_3 + \phi_4''q_4 + \phi_5''q_5)], \tag{23a}$$

$$F_z^{m_c} = m_c[g\cos\theta - (\phi_3\ddot{q}_3 + \phi_4\ddot{q}_4 + \phi_5\ddot{q}_5) - 2V(\phi_3'\dot{q}_3 + \phi_4'\dot{q}_4 + \phi_5'\dot{q}_5) - V^2(\phi_3''q_3 + \phi_4''q_4 + \phi_5''q_5)], \tag{23b}$$

$$M_y^{m_c} = \frac{h}{2}\{-m_c[(\phi_1\ddot{q}_1 + \phi_2\ddot{q}_2) - \frac{h}{2}(\phi_6\ddot{q}_6 + \phi_7\ddot{q}_7)] - m_c g\sin\theta - \mu m_c[g\cos\theta - (\phi_3\ddot{q}_3 + \phi_4\ddot{q}_4 + \phi_5\ddot{q}_5) - 2V(\phi_3'\dot{q}_3 + \phi_4'\dot{q}_4 + \phi_5'\dot{q}_5) - V^2(\phi_3''q_3 + \phi_4''q_4 + \phi_5''q_5)]\}. \tag{23c}$$

The equivalent nodal forces of the inclined moving mass element are given by (See Fig. 2)

$$f_k = \phi_k F_x^{m_c} \quad (k = 1,2), \tag{24a}$$

$$f_k = \phi_k F_z^{m_c} \quad (k = 3,4,5), \tag{24b}$$

$$f_k = \phi_k M_y^{m_c} \quad (k = 6,7). \tag{24c}$$

By substituting Eq. (23) into Eq. (24)

$$\begin{Bmatrix} f_1 \\ f_2 \\ f_3 \\ f_4 \\ f_5 \\ f_6 \\ f_7 \end{Bmatrix} = m_c g \begin{Bmatrix} -\phi_1(\mu\cos\theta + \sin\theta) \\ -\phi_2(\mu\cos\theta + \sin\theta) \\ \phi_3\cos\theta \\ \phi_4\cos\theta \\ \phi_5\cos\theta \\ -\phi_6\frac{h}{2}(\mu\cos\theta + \sin\theta) \\ -\phi_7\frac{h}{2}(\mu\cos\theta + \sin\theta) \end{Bmatrix} - m_c \begin{Bmatrix} \phi_1[\phi_1\ddot{q}_1 + \phi_2\ddot{q}_2 - \frac{h}{2}(\phi_6\ddot{q}_6 + \phi_7\ddot{q}_7) - \mu(\phi_3\ddot{q}_3 + \phi_4\ddot{q}_4 + \phi_5\ddot{q}_5)] \\ \phi_2[\phi_1\ddot{q}_1 + \phi_2\ddot{q}_2 - \frac{h}{2}(\phi_6\ddot{q}_6 + \phi_7\ddot{q}_7) - \mu(\phi_3\ddot{q}_3 + \phi_4\ddot{q}_4 + \phi_5\ddot{q}_5)] \\ \phi_3(\phi_3\ddot{q}_3 + \phi_4\ddot{q}_4 + \phi_5\ddot{q}_5) \\ \phi_4(\phi_3\ddot{q}_3 + \phi_4\ddot{q}_4 + \phi_5\ddot{q}_5) \\ \phi_5(\phi_3\ddot{q}_3 + \phi_4\ddot{q}_4 + \phi_5\ddot{q}_5) \\ \phi_6\frac{h}{2}[\phi_1\ddot{q}_1 + \phi_2\ddot{q}_2 - \frac{h}{2}(\phi_6\ddot{q}_6 + \phi_7\ddot{q}_7) - \mu(\phi_3\ddot{q}_3 + \phi_4\ddot{q}_4 + \phi_5\ddot{q}_5)] \\ \phi_7\frac{h}{2}[\phi_1\ddot{q}_1 + \phi_2\ddot{q}_2 - \frac{h}{2}(\phi_6\ddot{q}_6 + \phi_7\ddot{q}_7) - \mu(\phi_3\ddot{q}_3 + \phi_4\ddot{q}_4 + \phi_5\ddot{q}_5)] \end{Bmatrix} - 2Vm_c \begin{Bmatrix} -\phi_1\mu(\phi_3'\dot{q}_3 + \phi_4'\dot{q}_4 + \phi_5'\dot{q}_5) \\ -\phi_2\mu(\phi_3'\dot{q}_3 + \phi_4'\dot{q}_4 + \phi_5'\dot{q}_5) \\ \phi_3(\phi_3'\dot{q}_3 + \phi_4'\dot{q}_4 + \phi_5'\dot{q}_5) \\ \phi_4(\phi_3'\dot{q}_3 + \phi_4'\dot{q}_4 + \phi_5'\dot{q}_5) \\ \phi_5(\phi_3'\dot{q}_3 + \phi_4'\dot{q}_4 + \phi_5'\dot{q}_5) \\ -\phi_6\frac{h}{2}\mu(\phi_3'\dot{q}_3 + \phi_4'\dot{q}_4 + \phi_5'\dot{q}_5) \\ -\phi_7\frac{h}{2}\mu(\phi_3'\dot{q}_3 + \phi_4'\dot{q}_4 + \phi_5'\dot{q}_5) \end{Bmatrix} - m_c V^2 \begin{Bmatrix} -\phi_1\mu(\phi_3''q_3 + \phi_4''q_4 + \phi_5''q_5) \\ -\phi_2\mu(\phi_3''q_3 + \phi_4''q_4 + \phi_5''q_5) \\ \phi_3(\phi_3''q_3 + \phi_4''q_4 + \phi_5''q_5) \\ \phi_4(\phi_3''q_3 + \phi_4''q_4 + \phi_5''q_5) \\ \phi_5(\phi_3''q_3 + \phi_4''q_4 + \phi_5''q_5) \\ -\phi_6\frac{h}{2}\mu(\phi_3''q_3 + \phi_4''q_4 + \phi_5''q_5) \\ -\phi_7\frac{h}{2}\mu(\phi_3''q_3 + \phi_4''q_4 + \phi_5''q_5) \end{Bmatrix}. \tag{25}$$

Hence the motion equations of the moving mass element in matrix form are derived by the following equation

$$\{f\} = \{F\} - [m]\{\ddot{q}\}^e - [c]\{\dot{q}\}^e - [k]\{q\}^e, \tag{26}$$

where terms of $\{f\}$, $\{F\}$, $[m]$, $[c]$ and $[k]$ are given in Appendix B at the end of the paper. In Eqs. (23)-(25), ϕ_i, ϕ_i' and ϕ_i'' $(i = 1,...,7)$ must be calculated for $\varsigma = \varsigma_c$, in which ς_c denotes ς for the contact point.

3.5 Motion equations of the entire vibrating system

For including the effects of Coriolis and centrifugal accelerations of the moving mass in motion equations of the

entire vibrating system, the contribution of the mass, damping and stiffness matrices related to the moving mass element, $[m]$, $[c]$ and $[k]$, must be added to the each one of the corresponding overall matrices of the entire inclined FGM beam itself, $[M_b]$, $[C_b]$ and $[K_b]$. In other words, the time-dependent overall mass matrix $[M(t)]$, damping matrix $[C(t)]$ and stiffness matrix $[K(t)]$ of the entire vibrating system are obtained by

$$[M(t)]_{n\times n} = [M_b]_{n\times n} + [m]_{7\times 7}, \quad (27a)$$

$$[C(t)]_{n\times n} = [C_b]_{n\times n} + [c]_{7\times 7}, \quad (27b)$$

$$[K(t)]_{n\times n} = [K_b]_{n\times n} + [k]_{7\times 7}, \quad (27c)$$

$$M_{ij} = M_{b,ij} \ (i,j = 1,\ldots,n \text{ except: } i,j = s_k (k = 1,..7)), \quad (27d)$$

$$C_{ij} = C_{b,ij} \ (i,j = 1,\ldots,n \text{ except: } i,j = s_k (k = 1,..7)), \quad (27e)$$

$$K_{ij} = K_{b,ij} \ (i,j = 1,\ldots,n \text{ except: } i,j = s_k (k = 1,..7)), \quad (27f)$$

$$M_{s_k s_p} = M_{b,s_k s_p} + \mathrm{m_{kp}} \ (\mathrm{k,\ p} = 1,\ldots,7), \quad (27g)$$

$$C_{s_k s_p} = C_{b,s_k s_p} + \mathrm{c_{kp}} \ (\mathrm{k,\ p} = 1,\ldots,7), \quad (27h)$$

$$K_{s_k s_p} = K_{b,s_k s_p} + \mathrm{k_{kp}} \ (\mathrm{k,\ p} = 1,\ldots,7), \quad (27i)$$

where the total degrees of freedom of the entire vibrating system is denoted by n, the subscript s_k $(k = 1,\ldots,7)$ represents the numbering of the 7 degrees of freedom of the moving mass element. Therefore, the motion equation of the entire vibrating system is given by

$$[M(t)]\{\ddot{q}(t)\} + [C(t)]\{\dot{q}(t)\} + [K(t)]\{q(t)\} = \{F(t)\}, \quad (28)$$

where

$$\{F(t)\}_{n\times 1} = \{Q\}_{n\times 1} + \{f\}_{7\times 1}, \quad (29a)$$

$$F_i = Q_i \ (\mathrm{i} = 1,\ldots,\ \mathrm{n \ \ except \ \ i} = \mathrm{s_k}(k = 1,\ldots 7)), \quad (29b)$$

$$F_{s_i} = Q_{s_i} + f_{\mathrm{i}} \ \ (\mathrm{i} = 1,\ldots,7). \quad (29c)$$

4. Numerical results and discussion

In the numerical results, forced vibration of the inclined FGM beam is investigated with the different boundary conditions. The material of the FGM beam is composed of Steel (SUS304) and Alumina (Al_2O_3), which their properties are shown in Table 1, and its properties vary along the thickness direction of the beam according to the power-law distribution. The bottom surface of the FGM beam is pure Alumina, whereas the top surface of the beam is pure Steel. The dimensions and material properties of the studied inclined FGM beam in this paper are as follows. The beam thickness $h = 0.072322$ m, the beam width $b = 0.018113$ m, the length of the beam $L = 4.352$ m and the damping ratios $\zeta_1 = \zeta_2 = 0.005$. The moving mass $m_c = 4.6$ kg, the friction coefficient between the beam and the moving mass $\mu = \tan\theta$, and all of the present numerical results were acquired based on the acceleration of gravity $g = 9.81\mathrm{m/s^2}$. The responses of the system in each time step are obtained by applying the average acceleration scheme from the Newmark's time integration family procedures. The number of time steps is 100, and the finite element model of the inclined FGM beam is assembled of 80 identical beam elements. The dimensionless transverse displacements of the inclined beam are obtained by the mid-point static deflection of the simply-supported horizontal fully Steel (SUS304) beam under a concentrated shear force $m_c g$ at this point, $D = m_c g L^3 / 48EI$. For convenience, in the numerical results, T and T_c denote the total time taken by traversing the moving mass from the left end of the beam to the right end and the time that the maximum transverse displacement of the beam mid-point occurs in it, respectively. Furthermore, $w_{\max}$ and V_c indicate the maximum transverse displacement of the beam and a moving mass speed leading to the maximum transverse deflection of the beam, which is called the critical velocity, respectively. In general, there is a difference between the critical velocity and the fundamental velocity, the fundamental velocity for a beam is calculated based on its fundamental frequency.

Table 1 Material property of FGM constituents

Property	Unit	Stainless steel (SUS304)	Alumina (Al_2O_3)	Aluminum (Al)
E	GPa	210	390	70
ρ	$\mathrm{kg/m^3}$	8166	3960	2700
ν	-	0.3177	0.3	0.3

4.1 Validation

The numerical results of the free vibration analysis for the FGM beam in the limit cases are given in order to assess the accuracy and validity of the present formulation and numerical results. To that end, the first non-dimensional natural frequencies of the FGM beam with different boundary conditions $(\lambda = (\omega L^2 / h)\sqrt{\rho_m / E_m})$ are shown in Table 2, where $\rho_m = \int_{-h/2}^{h/2} \rho(z)dz$ and $E_m = \int_{-h/2}^{h/2} E(z)dz$. It is assumed that the FGM beam is made from the mixture of Aluminum (Al) and Alumina and their volume fractions vary through the thickness of the beam according to the power-law expression. The results of this free vibration analysis are compared with the results of

Table 2 Non-dimensional fundamental frequency for the FGM beam with different boundary conditions, different length-to-height ratios and $k = 0.3$

Boundary Conditions	Theory	L/h = 100	L/h = 30	L/h = 10
Simply-supported	FSDBT1 [Sina *et al.*]	2.817	2.813	2.774
	FSDBT2 [Sina *et al.*]	2.742	2.737	2.695
	Present (FSDBT)	2.778	2.773	2.734
Clamped-Clamped	FSDBT1 [Sina *et al.*]	6.384	6.343	6.013
	FSDBT2 [Sina *et al.*]	6.212	6.167	5.811
	Present (FSDBT)	6.211	6.171	5.851
Clamped-Free	FSDBT1 [Sina *et al.*]	1.003	1.003	0.996
	FSDBT2 [Sina *et al.*]	0.977	0.976	0.969
	Present (FSDBT)	0.977	0.976	0.969

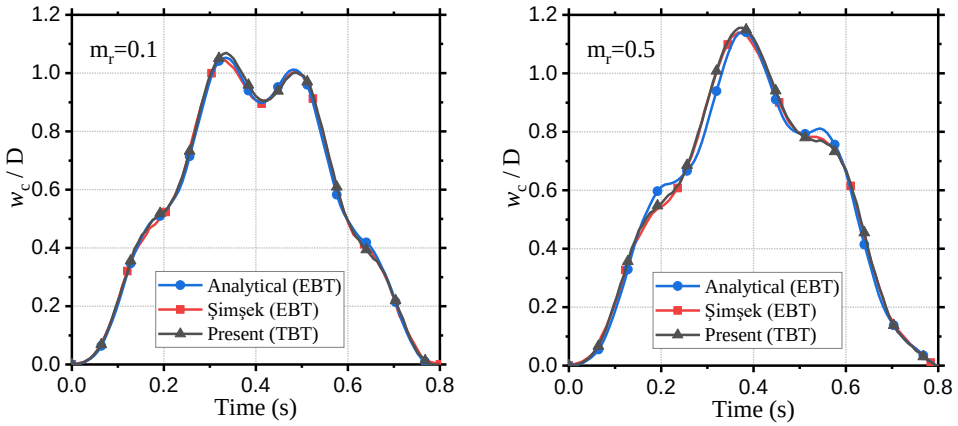

Fig. 3 The dimensionless transverse displacements of the contact point for the horizontal fully steel beam, $V = 25\,m/s$, $L/h = 20$ and $m_r = 0.1, 0.5$

different theories (Sina *et al.* 2009). A fast convergence rate of the results and their close accordance with those derived by the other studies, in all cases, validate the present formulation and numerical results.

For validate the present dynamic solution, the material of the beam is considered to be full Steel (SUS304), and the effects of Coriolis and centrifugal accelerations of the moving mass on the dynamic responses of the beam are neglected. In Fig. 3, the results for the dimensionless transverse displacements of the contact point, in other words, the dimensionless moving mass trajectory, are plotted for the beam width $b = 0.5\,\text{m}$, the beam thickness $h = 1\,\text{m}$, the beam length $L = 20\,\text{m}$, the speed of the moving mass $V = 25\,\text{m/s}$ and different mass ratios, which the mass ratio is taken as $m_r = m_c / M_{beam}$. The comparisons show that the agreement of the present study with the analytical solution of the simply-supported horizontal beam based on the Euler-Bernoulli theory (EBT) (Stanišić and Hardin 1969) and the results reported by Şimşek (2010) is excellent.

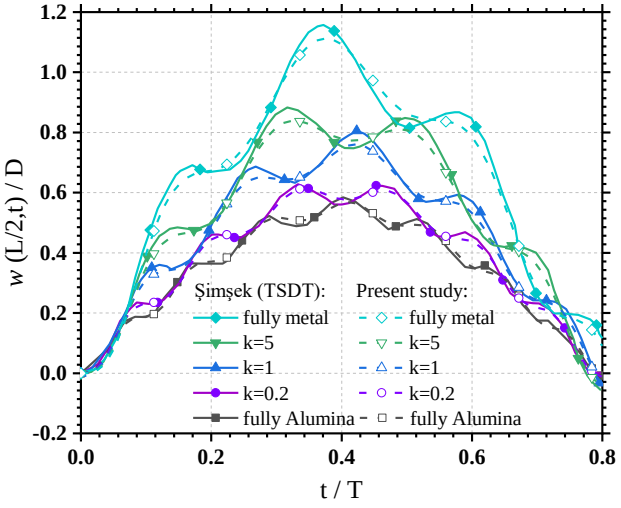

Fig. 4 The time history of the dimensionless transverse displacements at the mid-point of the simply-supported horizontal FGM beam for different material indices, $V = 25\,m/s$, $L/h = 20$ and $m_r = 0.5$

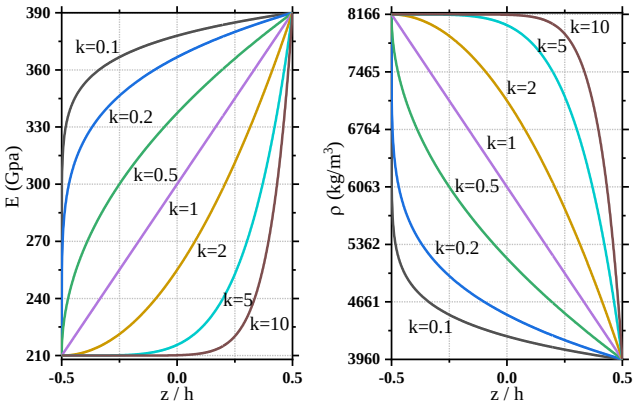

Fig. 5 The variations of the Young's modulus and the mass density through the FGM beam thickness

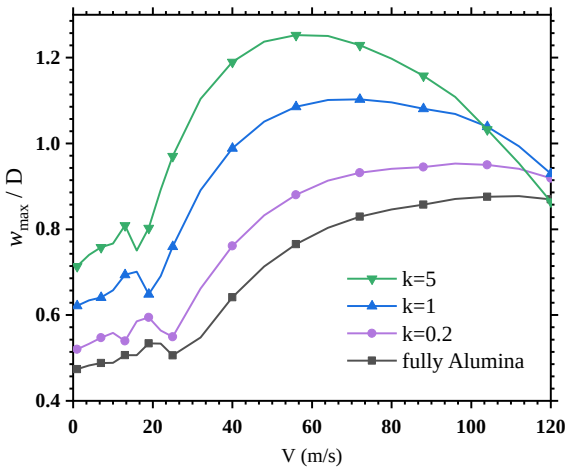

Fig. 6 The dimensionless maximum transverse displacement of the simply-supported inclined FGM beam with respect to the velocity of the moving mass for different material indices

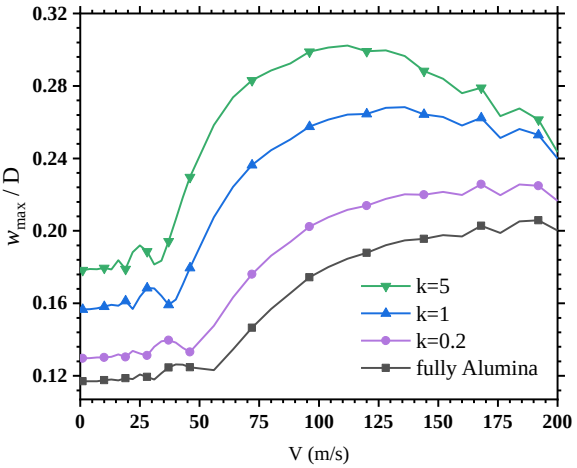

Fig. 7 The dimensionless maximum transverse displacement of the clamped-clamped inclined FGM beam with respect to the velocity of the moving mass for different material indices

Moreover, in order to more validate the present formulation and numerical results, in Fig. 4, the time history of the dimensionless mid-point transverse displacement is plotted for $L/h=20$, $m_r=0.5$, $V=25$ m/s and different material indices k. The effects of Coriolis and centrifugal accelerations of the moving mass on the dynamic responses of the horizontal FGM beam are considered. As can be seen, there is a good accord between the results of the present study and the results of third-order shear deformation theory (TSDT) reported by Şimşek (2010).

4.2 Effects of power-law index

In Fig. 5, variations of the Young's modulus and the mass density through the beam thickness are shown for the various material indices, according to the power-law distribution. By increasing the material index, the relative volume of the steel used in the FGM beam increases, hence, as shown in Fig. 5, the Young's modulus and the mass density of the FGM beam decreases and increases, respectively.

In Figs. 6 and 7, the variation of dimensionless w_{max} with respect to the velocity of the moving mass is plotted for an inclined FGM beam with the clamped-clamped and simply-supported boundary conditions and different material indices. As can be seen, the dimensionless w_{max} of the clamped-clamped and simply-supported inclined FGM beams can be divided into two regions: under-critical and over-critical regions, and for both of these regions, by increasing the material index, w_{max} and V_c increases and decreases, respectively.

The dimensionless mid-point transverse displacement of the simply-supported inclined FGM beam for the under-critical, over-critical velocities of the moving mass and different material indices of the FGM beam is plotted in Figs. 8-9, and that obtained for the clamped-clamped inclined FGM beam is shown in Figs. 10 and 11. It can be concluded that the maximum transverse displacement of the mid-point of the simply-supported and clamped-clamped inclined FGM beams has a time-delay respective to the position of the moving mass when the velocity is in the over-critical region, and this tendency cannot always be observed in the under-critical region. As one can see, for an FGM beam traversed by a mass with an over-critical velocity, T_c increases with increasing the material index; in other words, the time-delay increases by decreasing the beam stiffness. Also, for the over-critical velocities of the moving mass, the maximum deflection of the beam mid-point may occur after or before the moving mass leaving the right end of the beam, while for the under-critical velocities of the moving mass, it happens before the moving mass leaving the right end of the beam ($T_c<T$). Moreover, in the under-critical region, for cases that $T_c>T/2$, the time-delay respective to the position of the moving mass increases with increasing the material index.

4.3 Effects of Coriolis and centrifugal accelerations

In Fig. 12, the dimensionless w_{max} for the inclined FGM beam with the clamped-clamped and simply-supported boundary conditions and different material indices is plotted with respect to the velocity of the moving mass. As can be observed, for all studied cases, both w_{max} and V_c increase by considering the centrifugal acceleration, while both of them decrease by considering the Coriolis acceleration. The influence of Coriolis and centrifugal accelerations on the dynamic behaviour of the inclined FGM beams increases with the increase of the moving mass velocity. On the other hand, the results obtained by simultaneously neglecting Coriolis and centrifugal accelerations are in much better agreement with those acquired by simultaneously considering both of these accelerations rather than those obtained by taking only one of them into account since these accelerations undermine the effects of each other on the dynamic behaviour of the inclined FGM beam. The considering of the Coriolis and centrifugal accelerations simultaneously, in comparison with neglecting both of these accelerations simultaneously, leads to decrease and increase in the critical velocity for the clamped-clamped and simply-supported inclined FGM beams, respectively.

The dimensionless mid-point transverse displacement of the clamped-clamped and simply-supported inclined FGM beams for the under-critical, over-critical velocities of the moving mass and the different material indices of the FGM beam is plotted in Fig. 13. As it is seen, for all investigated

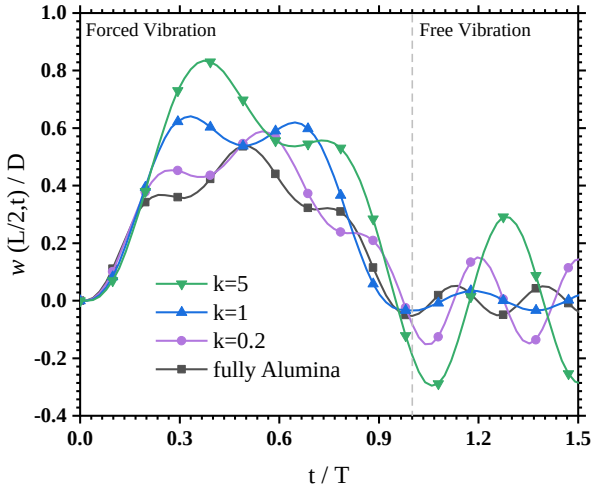

Fig. 8 The time history of the dimensionless transverse displacement at the mid-point of the simply-supported inclined FGM beam for different material indices, $V = 20\ m/s$

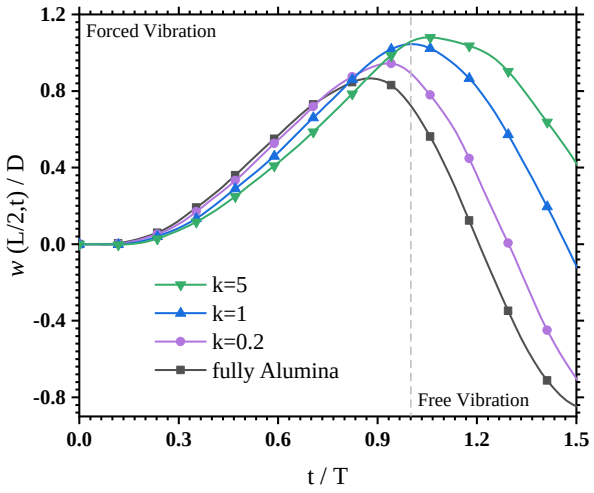

Fig. 9 The time history of the dimensionless transverse displacement at the mid-point of the simply-supported inclined FGM beam for different material indices, $V = 100\ m/s$

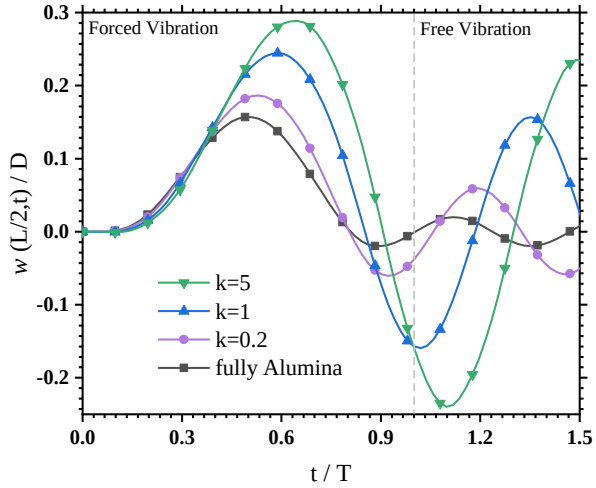

Fig. 10 The time history of the dimensionless transverse displacement at the mid-point of the clamped-clamped inclined FGM beam for different material indices, $V = 80\ m/s$

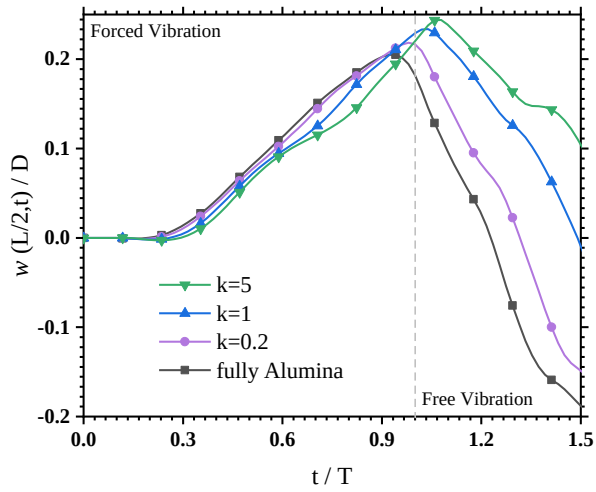

Fig. 11 The time history of the dimensionless transverse displacement at the mid-point of the clamped-clamped inclined FGM beam for different material indices, $V = 230\ m/s$

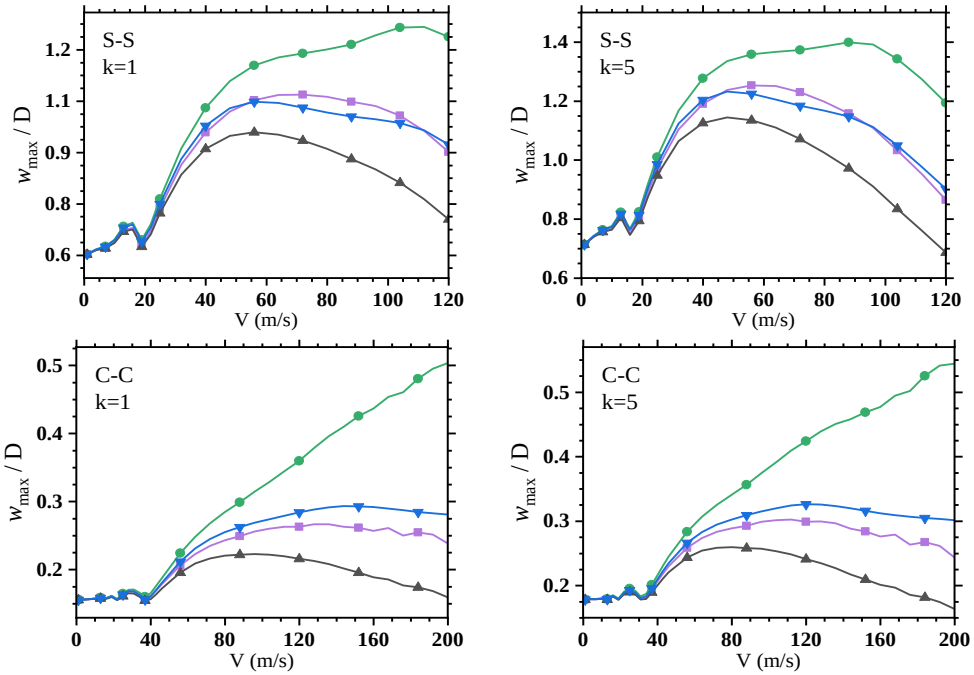

Fig. 12 The dimensionless maximum transverse displacement of the simply-supported (S-S) and clamped-clamped (C-C) inclined FGM beams with respect to the velocity of the moving mass for $k=1,5$, with considering centrifugal acceleration (—●—), with considering Coriolis acceleration (—▲—), with considering Coriolis and centrifugal accelerations simultaneously (—■—), with neglecting Coriolis and centrifugal accelerations simultaneously (—▼—)

cases, the vibration amplitude of the inclined FGM beam mid-point decreases when both effects of the Coriolis and centrifugal accelerations are considered simultaneously. The influence of considering both of the accelerations for the high speeds of the moving mass is much greater in comparison with that for the low speeds because according to Eq. (19b) the magnitude of the Coriolis and centrifugal accelerations are proportional to the moving mass speed and square of it, respectively. Hence, the Coriolis and centrifugal accelerations can be neglected for a beam traversed by a low-speed mass.

4.4 Effects of the inclined angle

In Fig. 14, the dimensionless w_{max} with respect to the velocity of the moving mass is plotted for the clamped-clamped and simply-supported inclined FGM beams, which the results are computed for the different material indices and the different inclined angles of the beam with respect to the horizon. As one can observe, for all examined cases, w_{max} decreases by increasing the inclined angle of the beam.

In Fig. 15, the time history of the dimensionless mid-point transverse displacement is plotted for the clamped-clamped and simply-supported inclined FGM beams under the moving mass with the under-critical and over-critical velocities, which the results are calculated for the different material indices and the different inclined angles of the beam. As can be seen, for all investigated cases, by increasing the inclined angle of the inclined FGM beam, the vibration amplitude of the beam mid-point decreases, because of the decrease in the transverse component of the moving mass weight.

5. Conclusions

The dynamic behaviour of an inclined functionally graded material beam with different boundary conditions under a moving mass is investigated based on the first-order shear deformation theory. The material properties of the FGM beam vary continuously, based on the power-law distribution along the beam thickness. The moving mass is considered on the top surface of the beam instead of supposing it on the mid-plane of the beam. The comparisons show that the agreement of the present results with those in the existing literature is excellent. The effects of the boundary conditions, the moving mass velocity, various material distributions, inclined angle of the beam, Coriolis and centrifugal accelerations of the moving mass are studied. In this paper for the first time in dynamic analysis of the inclined FGM beams, the Coriolis and centrifugal accelerations of the moving mass are taken into account. The new provided results for dynamics of the inclined FGM beams traversed by a moving mass can be significant for the scientific and engineering community in the area of FGM structures. Based on the present results, one may draw the following conclusions:

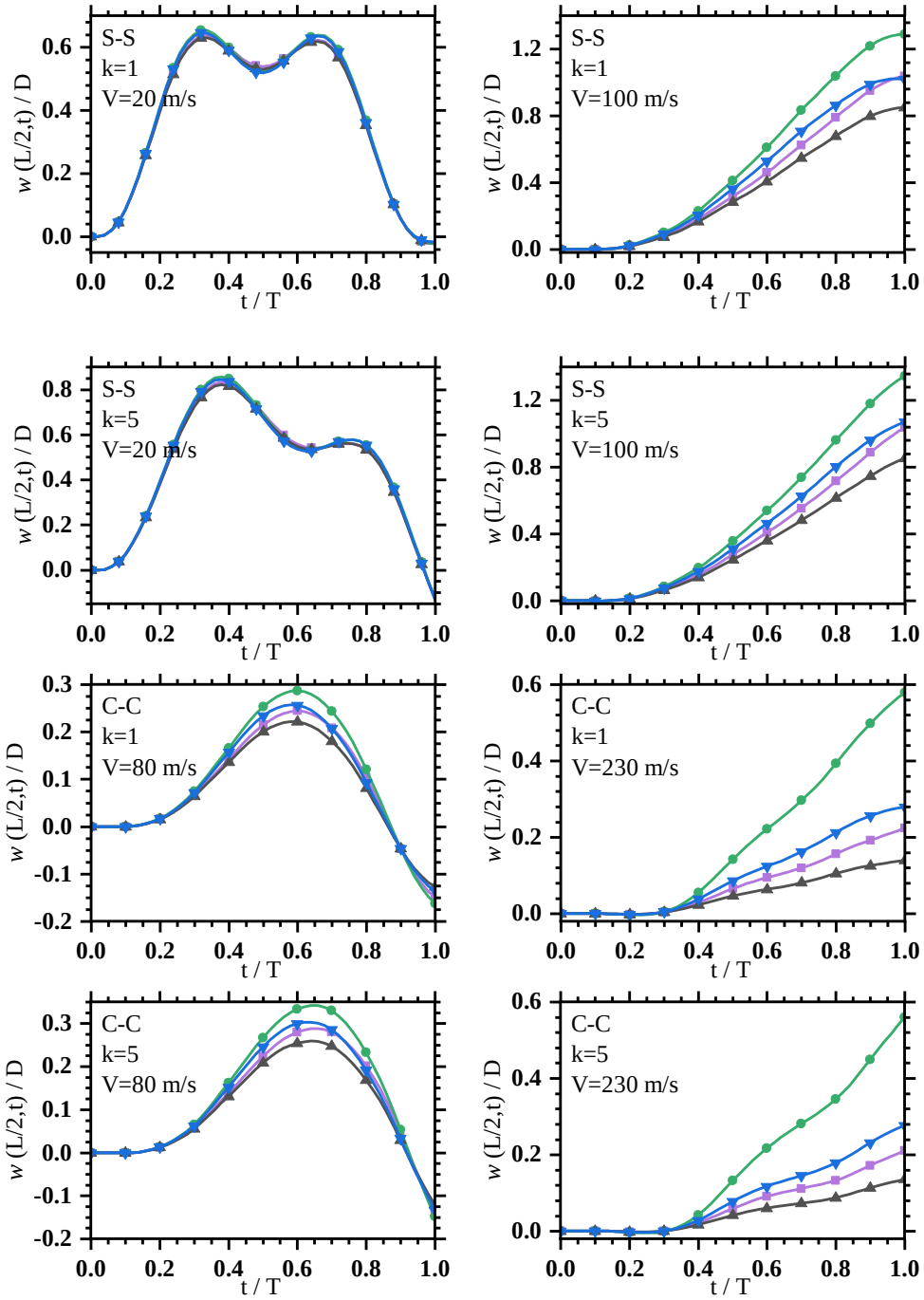

Fig. 13 The time history of the dimensionless transverse displacement at the mid-point of the simply-supported (S-S) and clamped-clamped (C-C) inclined FGM beams for $k = 1, 5$, different velocities of the moving mass, with considering centrifugal acceleration (—●—), with considering Coriolis acceleration (—▲—), with considering Coriolis and centrifugal accelerations simultaneously (—■—), with neglecting Coriolis and centrifugal accelerations simultaneously (—▼—)

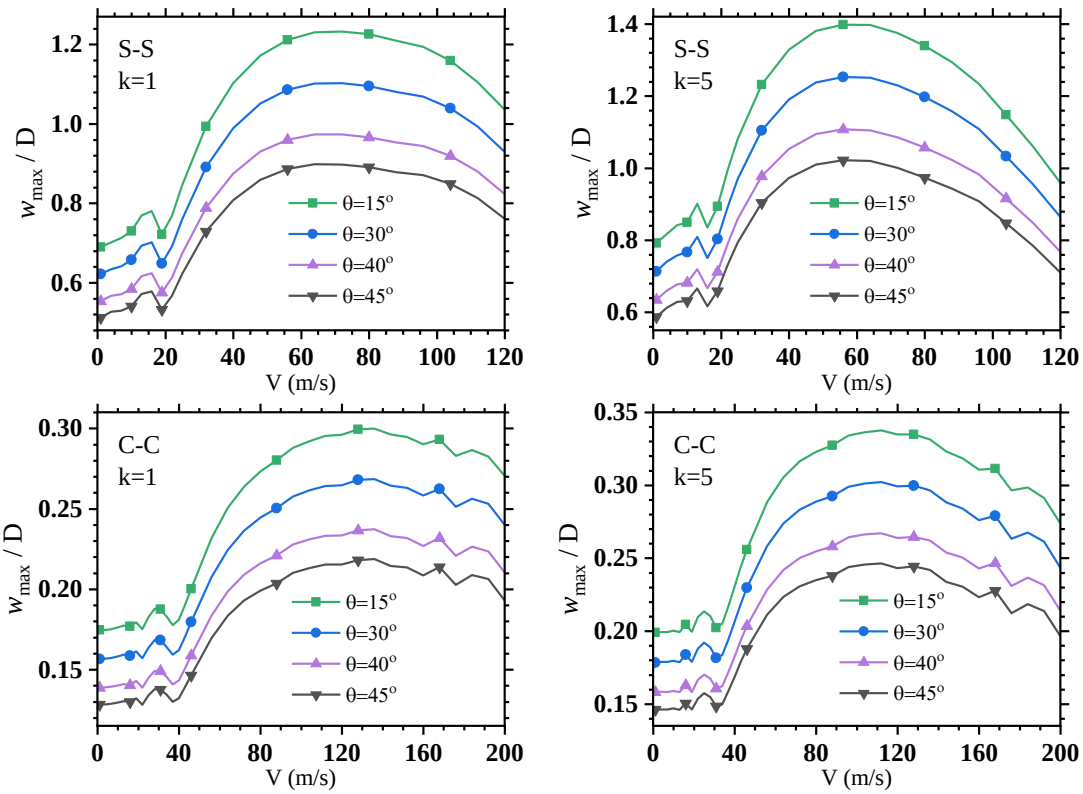

Fig. 14 The dimensionless maximum transverse displacement of the simply-supported (S-S) and clamped-clamped (C-C) inclined FGM beams with respect to the velocity of the moving mass for $k=1,5$ and different inclined angle of the beam with respect to the horizon

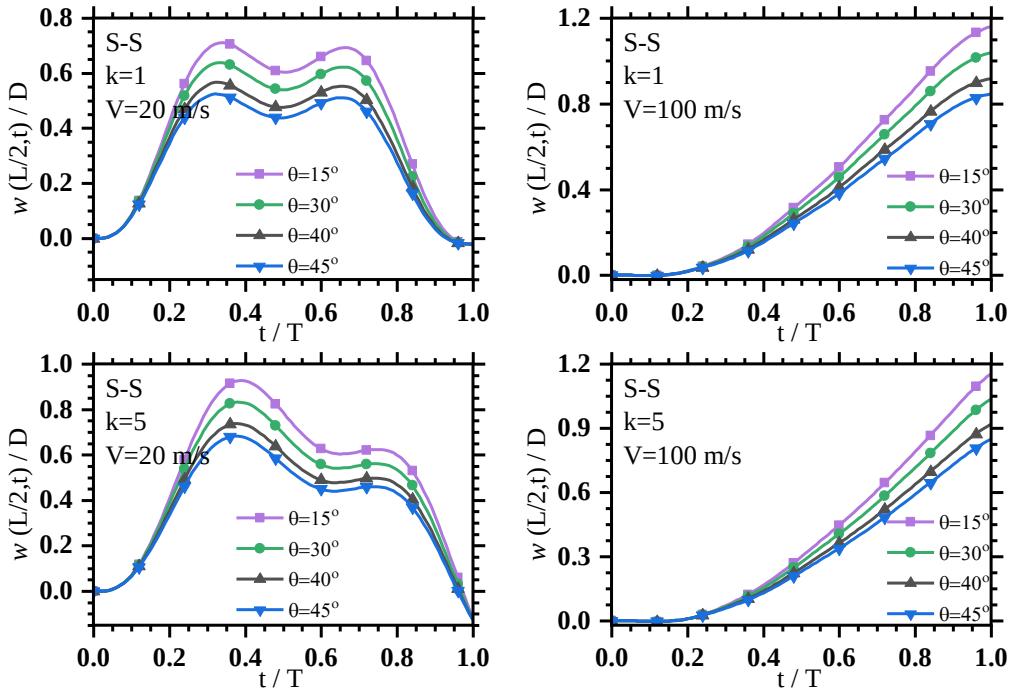

Continued-

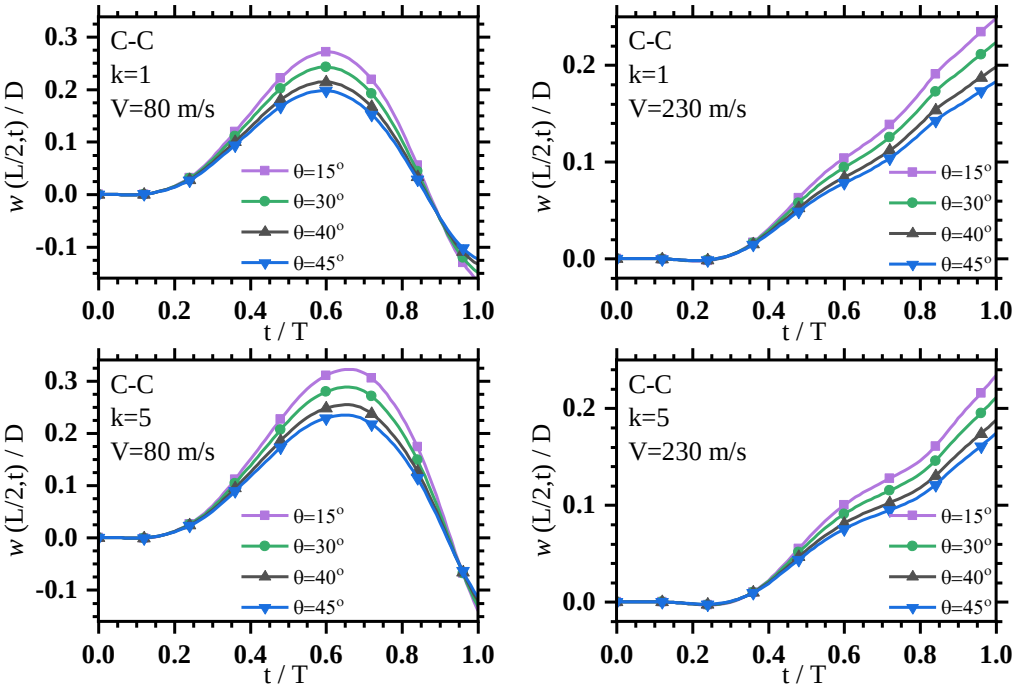

Fig. 15 The time history of the dimensionless transverse displacement at the mid-point of the simply-supported (S-S) and clamped-clamped (C-C) inclined FGM beams for different velocities of the moving mass, different inclined angle of the beam with respect to the horizon and $k=1,5$

- For the under-critical and over-critical velocities of the moving mass, by increasing the material index, $w_{\max}$ and V_c increases and decreases, respectively.
- The maximum transverse displacement of the mid-point of the simply-supported and clamped-clamped inclined FGM beams has a time-delay respective to the position of the moving mass when the velocity is in the over-critical region, and this tendency cannot always be observed in the under-critical region.
- For the over-critical velocities of the moving mass, the maximum deflection of the beam mid-point may occur after or before the moving mass leaving the right end of the beam, while for the under-critical velocities of the moving mass, it happens before the moving mass leaving the right end of the beam ($T_c < T$).
- For an FGM beam traversed by a mass with an over-critical velocity, T_c increases with increasing the material index; in other words, the time-delay respective to the position of the moving mass increases by decreasing the beam stiffness. Moreover, in the under-critical region, for cases that $T_c > T/2$, the time-delay increases with increasing the material index.
- By considering the centrifugal acceleration in the dynamic analysis of an inclined FGM beam traversed by a moving mass, both $w_{\max}$ and V_c increase, while both of them decrease by considering the Coriolis acceleration.
- The influence of Coriolis and centrifugal accelerations on the dynamic behaviour of the inclined FGM beams increases with the increase of the moving mass velocity.
- The results obtained by simultaneously neglecting Coriolis and centrifugal accelerations are in much better agreement with those acquired by simultaneously considering both of these accelerations rather than those obtained by taking only one of them into account since these accelerations undermine the effects of each other on the dynamic behaviour of the inclined FGM beam.
- The considering of the Coriolis and centrifugal accelerations simultaneously, in comparison with neglecting both of these accelerations simultaneously, leads to decrease and increase in the critical velocity for the clamped-clamped and simply-supported inclined FGM beams, respectively.
- The vibration amplitude of the inclined FGM beam mid-point decreases when both effects of the Coriolis and centrifugal accelerations are considered simultaneously.
- The influence of considering both the Coriolis and centrifugal accelerations for the high speeds of the moving mass is much greater in comparison with that for the low speeds because according to Eq. (19b) the magnitude of the Coriolis and centrifugal accelerations are proportional to the moving mass speed and square of it, respectively. Hence, the Coriolis and centrifugal accelerations can be neglected for a beam traversed by a low-speed mass.
- By increasing the inclined angle of the FGM beams with respect to the horizon, $w_{\max}$ and the vibration amplitude of the beam mid-point decrease, because of the

decrease in the transverse component of the moving mass weight.

References

Arioui, O., Belakhdar, K., Kaci, A. and Tounsi, A. (2018), "Thermal buckling of FGM beams having parabolic thickness variation and temperature dependent materials", *Steel Compos. Struct.*, **27**(6), 777-788. https://doi.org/10.12989/scs.2018.27.6.777.

Bathe, K. (1982), *Finite Element Procedures in Engineering Analysis*, Prentice-Hall, Englewood Cliffs, NJ, USA.

Benferhat, R., Hassaine Daouadji, T., Hadji, L. and Said Mansour, M. (2016), "Static analysis of the FGM plate with porosities", *Steel Compos. Struct.*, **21**(1), 123-136. https://doi.org/10.12989/scs.2016.21.1.123.

Bourada, M., Kaci, A., Houari, M.S.A. and Tounsi, A. (2015), "A new simple shear and normal deformations theory for functionally graded beams", *Steel Compos. Struct.*, **18**(2), 409-423. https://doi.org/10.12989/scs.2015.18.2.409.

Burlayenko, V., Altenbach, H., Sadowski, T., Dimitrova, S. and Bhaskar, A. (2017), "Modelling functionally graded materials in heat transfer and thermal stress analysis by means of graded finite elements", *Appl. Math. Model.*, **45**, 422-438. https://doi.org/10.1016/j.apm.2017.01.005.

Chaht, F.L., Kaci, A., Houari, M.S.A., Tounsi, A., Bég, O.A. and Mahmoud, S. (2015), "Bending and buckling analyses of functionally graded material (FGM) size-dependent nanoscale beams including the thickness stretching effect", *Steel Compos. Struct.*, **18**(2), 425-442. https://doi.org/10.12989/scs.2015.18.2.425.

Chen, C.S., Liu, F.H. and Chen, W.R. (2017), "Vibration and stability of initially stressed sandwich plates with FGM face sheets in thermal environments", *Steel Compos. Struct.*, **23**(3), 251-261. https://doi.org/10.12989/scs.2017.23.3.251.

Cho, J. (2019), "Computation of mixed-mode stress intensity factors in functionally graded materials by natural element method", *Steel Compos. Struct.*, **31**(1), 43-51. https://doi.org/10.12989/scs.2019.31.1.043.

Cicirello, A. (2019), "On the response bounds of damaged Euler–Bernoulli beams with switching cracks under moving masses", *Int. J. Solids Struct.*, **172-173**, 70-83. https://doi.org/10.1016/j.ijsolstr.2019.05.003.

Cifuentes, A.O. (1989), "Dynamic response of a beam excited by a moving mass", *Finite Elem. Anal. Des.*, **5**(3), 237-246. https://doi.org/10.1016/0168-874X(89)90046-2.

Darilmaz, K. (2015), "Vibration analysis of functionally graded material (FGM) grid systems", *Steel Compos. Struct.*, **18**(2), 395-408. https://doi.org/10.12989/scs.2015.18.2.395.

Dimitrovová, Z. (2019), "Semi-analytical solution for a problem of a uniformly moving oscillator on an infinite beam on a two-parameter visco-elastic foundation", *J. Sound Vib.*, **438**, 257-290. https://doi.org/10.1016/j.jsv.2018.08.050.

Duy, H.T., Van, T.N. and Noh, H.C. (2014), "Eigen analysis of functionally graded beams with variable cross-section resting on elastic supports and elastic foundation", *Struct. Eng. Mech.*, **52**(5), 1033-1049. https://doi.org/10.12989/sem.2014.52.5.1033.

Dyniewicz, B., Bajer, C., Kuttler, K. and Shillor, M. (2019), "Vibrations of a Gao beam subjected to a moving mass", *Nonlinear Analysis: Real World Applications*. **50**, 342-364. https://doi.org/10.1016/j.nonrwa.2019.05.007.

Esen, I. (2011), "Dynamic response of a beam due to an accelerating moving mass using moving finite element approximation", *Math. Comput.l Appl.*, **16**(1), 171-182. https://doi.org/10.3390/mca16010171.

Esen, I. (2019), "Dynamic response of a functionally graded Timoshenko beam on two-parameter elastic foundations due to a variable velocity moving mass", *Int. J. Mech. Sci.*, **153**, 21-35. https://doi.org/10.1016/j.ijmecsci.2019.01.033.

Esen, I. and Koç, M.A. (2015), "Dynamic response of a 120 mm smoothbore tank barrel during horizontal and inclined firing positions", *Latin Am. J. Solids Struct.*, **12**(8), 1462-1486. https://doi.org/10.1590/1679-78251576.

Esen, I., Koc, M.A. and Cay, Y. (2018), "Finite element formulation and analysis of a functionally graded Timoshenko beam subjected to an accelerating mass including inertial effects of the mass", *Latin Am. J. Solid. Struct.*, **15**(10). https://doi.org/10.1590/1679-78255102.

Froio, D., Rizzi, E., Simões, F.M. and Da Costa, A.P. (2018), "Dynamics of a beam on a bilinear elastic foundation under harmonic moving load", *Acta Mechanica*, **229**(10), 4141-4165. https://doi.org/10.1007/s00707-018-2213-4.

Greco, F. and Lonetti, P. (2018), "Numerical formulation based on moving mesh method for vehicle–bridge interaction", *Adv. Eng. Softw.*, **121**, 75-83. https://doi.org/10.1016/j.advengsoft.2018.03.013.

Hoang, T., Duhamel, D., Forêt, G., Yin, H.P., Joyez, P. and Caby, R. (2017), "Calculation of force distribution for a periodically supported beam subjected to moving loads", *J. Sound Vib.*, **388**, 327-338. https://doi.org/10.1016/j.jsv.2016.10.031..

Horii, H. and Nemat-Nasser, S. (1985), "Elastic fields of interacting inhomogeneities", *Int. J. Solids Struct.*, **21**(7), 731-745. https://doi.org/10.1016/0020-7683(85)90076-9.

Hou, Z., Xia, H., Wang, Y., Zhang, Y. and Zhang, T. (2015), "Dynamic analysis and model test on steel-concrete composite beams under moving loads", *Steel Compos. Struct.*, **18**(3), 565-582. https://doi.org/10.12989/scs.2015.18.3.565.

Ichikawa, M., Miyakawa, Y. and Matsuda, A. (2000), "Vibration analysis of the continuous beam subjected to a moving mass", *J. Sound Vib.*, **230**(3), 493-506. https://doi.org/10.1006/jsvi.1999.2625.

Kadivar, M. and Mohebpour, S. (1998), "Forced vibration of unsymmetric laminated composite beams under the action of moving loads", *Compos. Sci. Technol.*, **58**(10), 1675-1684. https://doi.org/10.1016/S0266-3538(97)00238-8.

Kar, V.R. and Panda, S.K. (2015), "Nonlinear flexural vibration of shear deformable functionally graded spherical shell panel", *Steel Compos. Struct.*, **18**(3), 693-709. https://doi.org/10.12989/scs.2015.18.3.693.

Kim, J. and Reddy, J. (2013), "Analytical solutions for bending, vibration, and buckling of FGM plates using a couple stress-based third-order theory", *Compos. Struct.*, **103**, 86-98. https://doi.org/10.1016/j.compstruct.2013.03.007.

Kocaturk, T. and Akbas, S.D. (2013), "Thermal post-buckling analysis of functionally graded beams with temperature-dependent physical properties" *Steel Compos. Struct.*, **15**(5), 481-505. https://doi.org/10.12989/scs.2013.15.5.481.

Kourehli, S.S., Ghadimi, S. and Ghadimi, R. (2018), "Crack identification in Timoshenko beam under moving mass using RELM", *Steel Compos. Struct.*, **28**(3), 279-288. https://doi.org/10.12989/scs.2018.28.3.279.

Michaltsos, G., Sophianopoulos, D. and Kounadis, A. (1996), "The effect of a moving mass and other parameters on the dynamic response of a simply supported beam", *J. Sound Vib.,* **191**(3), 357-362. https://doi.org/10.1006/jsvi.1996.0127.

Miyamoto, Y., Kaysser, W., Rabin, B., Kawasaki, A. and Ford, R.G. (2013), *Functionally Graded Materials: Design, Processing and Applications*, Springer Science & Business Media, New York, NY, USA.

Mohebpour, S., Daneshmand, F. and Mehregan, H. (2013), "Numerical analysis of inclined flexible beam carrying one degree of freedom moving mass including centrifugal and

Coriolis accelerations and rotary inertia effects", *Mech. Based Des. Struct. Mach*., **41**(2), 123-145. https://doi.org/10.1080/15397734.2012.681592.

Mohebpour, S.R., Vaghefi, M. and Ezzati, M. (2016), "Numerical analysis of an inclined cross-ply laminated composite beam subjected to moving mass with consideration the Coriolis and centrifugal forces", *Eur. J. Mech. -A/Solids*, **59**, 67-75. https://doi.org/10.1016/j.euromechsol.2016.03.003.

Moleiro, F., Correia, V.F., Ferreira, A. and Reddy, J. (2019), "Fully coupled thermo-mechanical analysis of multilayered plates with embedded FGM skins or core layers using a layerwise mixed model", *Compos. Struct*., **210**, 971-996. https://doi.org/10.1016/j.compstruct.2018.11.073.

Nguyen, D.K. and Tran, T.T. (2018), "Free vibration of tapered BFGM beams using an efficient shear deformable finite element model", *Steel Compos. Struct.*, **29**(3), 363-377. https://doi.org/10.12989/scs.2018.29.3.363.

Shokouhifard, V., Mohebpour, S., Malekzadeh, P. and Golbaharhaghighi, M. (2019), "Inverse dynamic analysis of an inclined FGM beam due to moving load for estimating the mass of moving load based on a CGM", *Iranian J. Sci. Technol*., *T. Mech. Eng*., 1-14. https://doi.org/10.1007/s40997-019-00291-2.

Simsek, M. (2011), "Forced vibration of an embedded single-walled carbon nanotube traversed by a moving load using nonlocal Timoshenko beam theory", *Steel Compos. Struct.*, **11**(1), 59-76. https://doi.org/10.12989/scs.2011.11.1.059

Şimşek, M. (2010), "Vibration analysis of a functionally graded beam under a moving mass by using different beam theories", *Compos. Struct*., **92**(4), 904-917. https://doi.org/10.1016/j.compstruct.2009.09.030

Sina, S., Navazi, H. and Haddadpour, H. (2009), "An analytical method for free vibration analysis of functionally graded beams", *Mater. Design*, **30**(3), 741-747. https://doi.org/10.1016/j.matdes.2008.05.015

Song, M., Kitipornchai, S. and Yang, J. (2017), "Free and forced vibrations of functionally graded polymer composite plates reinforced with graphene nanoplatelets", *Compos. Struct*., **159**, 579-588. https://doi.org/10.1016/j.compstruct.2016.09.070

Stanišić, M.M. and Hardin, J.C. (1969), "On the response of beams to an arbitrary number of concentrated moving masses", *J. Franklin Inst*., **287**(2), 115-123. https://doi.org/10.1016/0016-0032(69)90120-3

Stojanović, V., Kozić, P. and Petković, M.D. (2017), "Dynamic instability and critical velocity of a mass moving uniformly along a stabilized infinity beam", *Int. J. Solids Struct*., **108**, 164-174. https://doi.org/10.1016/j.ijsolstr.2016.12.010

Suresh, S. and Mortensen, A. (1998), *Fundamentals of Functionally Graded Materials*, The Institut of Materials, London, England.

Thai, H.-T. and Vo, T.P. (2012), "Bending and free vibration of functionally graded beams using various higher-order shear deformation beam theories", *Int. J. Mech. Sci*., **62**(1), 57-66. https://doi.org/10.1016/j.ijmecsci.2012.05.014

Wu, J.-J. (2005), "Dynamic analysis of an inclined beam due to moving loads", *J. Sound Vib*., **288**(1-2), 107-131. https://doi.org/10.1016/j.jsv.2004.12.020

Wu, J.J. (2004), "Dynamic responses of a three-dimensional framework due to a moving carriage hoisting a swinging object", *Int. J. Numer. Method. E.,* **59**(13), 1679-1702. https://doi.org/10.1002/nme.916

Xu, X., Xu, W. and Genin, J. (1997), "A non-linear moving mass problem", *J. Sound Vib*., **204**(3), 495-504. https://doi.org/10.1006/jsvi.1997.0962

Appendix A

$$\left[M^{e}\right]=\begin{bmatrix} M_{ij}^{11} & M_{ij}^{12} & M_{ij}^{13} \\ M_{ij}^{21} & M_{ij}^{22} & M_{ij}^{23} \\ M_{ij}^{31} & M_{ij}^{32} & M_{ij}^{33} \end{bmatrix},\left[K^{e}\right]=\begin{bmatrix} K_{ij}^{11} & K_{ij}^{12} & K_{ij}^{13} \\ K_{ij}^{21} & K_{ij}^{22} & K_{ij}^{23} \\ K_{ij}^{31} & K_{ij}^{32} & K_{ij}^{33} \end{bmatrix},$$

$$M_{ij}^{11}=\int_0^l I_0\phi_i^{(1)}\phi_j^{(1)}dx \ \ (\mathrm{i},\ \mathrm{j}=1,2),$$
$$M_{ij}^{12}=0 \ \ (\mathrm{i}=1,2\ ,\ \mathrm{j}=1,2,3)\ ,$$
$$M_{ij}^{13}=\int_0^l I_1\phi_i^{(1)}\phi_j^{(3)}dx \ \ (\mathrm{i},\ \mathrm{j}=1,2),$$

$$M_{ij}^{21}=0 \ \ (\mathrm{i}=1,2,3\ ,\ \mathrm{j}=1,2),$$
$$M_{ij}^{22}=\int_0^l I_0\phi_i^{(2)}\phi_j^{(2)}dx \ \ (\mathrm{i},\ \mathrm{j}=1,2,3),$$
$$M_{ij}^{23}=0 \ \ (\mathrm{i}=1,2,3\ ,\ \mathrm{j}=1,2),$$

$$M_{ij}^{31}=\int_0^l I_1\phi_i^{(3)}\phi_j^{(1)}dx \ \ (\mathrm{i},\ \mathrm{j}=1,2),$$
$$M_{ij}^{32}=0 \ \ (\mathrm{i}=1,2\ ,\ \mathrm{j}=1,2,3),$$
$$M_{ij}^{33}=\int_0^l I_2\phi_i^{(3)}\phi_j^{(3)}dx \ \ (\mathrm{i},\ \mathrm{j}=1,2),$$

$$K_{ij}^{11}=\int_0^l A_{11}\frac{\partial\phi_i^{(1)}}{\partial x}\frac{\partial\phi_j^{(1)}}{\partial x}dx \ \ (\mathrm{i},\ \mathrm{j}=1,2),$$
$$K_{ij}^{12}=0 \ \ (\mathrm{i}=1,2\ ,\ \mathrm{j}=1,2,3),$$
$$K_{ij}^{13}=\int_0^l B_{11}\frac{\partial\phi_i^{(1)}}{\partial x}\frac{\partial\phi_j^{(3)}}{\partial x}dx \ \ (\mathrm{i},\ \mathrm{j}=1,2),$$

$$K_{ij}^{21}=0 \ \ (\mathrm{i}=1,2,3\ ,\ \mathrm{j}=1,2),$$
$$K_{ij}^{22}=\int_0^l k_s A_{55}\frac{\partial\phi_i^{(2)}}{\partial x}\frac{\partial\phi_j^{(2)}}{\partial x}dx \ \ (\mathrm{i},\ \mathrm{j}=1,2,3\ ),$$
$$K_{ij}^{23}=\int_0^l k_s A_{55}\frac{\partial\phi_i^{(2)}}{\partial x}\phi_j^{(3)}dx \ \ (\mathrm{i}=1,2,3\ ,\ \mathrm{j}=1,2),$$

$$K_{ij}^{31}=\int_0^l B_{11}\frac{\partial\phi_i^{(3)}}{\partial x}\frac{\partial\phi_j^{(1)}}{\partial x}dx \ \ (\mathrm{i},\ \mathrm{j}=1,2),$$
$$K_{ij}^{32}=\int_0^l k_s A_{55}\phi_i^{(3)}\frac{\partial\phi_j^{(2)}}{\partial x}dx \ \ (\mathrm{i}=1,2\ ,\ \mathrm{j}=1,2,3)$$

$$K_{ij}^{33}=\int_0^l D_{11}\frac{\partial\phi_i^{(3)}}{\partial x}\frac{\partial\phi_j^{(3)}}{\partial x}+k_s A_{55}\phi_i^{(3)}\phi_j^{(3)}dx \ \ (\mathrm{i},\ \mathrm{j}=1,2\ ) \quad \text{(A.1-20)}$$

and $Q_i^e \ \ (i=1,\ldots,7)$ are the nodal forces of an FGM beam element, which for two end nodes of the beam are zero or unknown, according to the boundary conditions.

Appendix B

$$\{f\}=\begin{bmatrix} f_1 & f_2 & f_3 & f_4 & f_5 & f_6 & f_7 \end{bmatrix}^T,$$

$$[m]=m_c\begin{bmatrix} m_{ij}^{11} & m_{ij}^{12} & m_{ij}^{13} \\ m_{ij}^{21} & m_{ij}^{22} & m_{ij}^{23} \\ m_{ij}^{31} & m_{ij}^{32} & m_{ij}^{33} \end{bmatrix},$$

$$[c]=2m_cV\begin{bmatrix} c_{ij}^{11} & c_{ij}^{12} & c_{ij}^{13} \\ c_{ij}^{21} & c_{ij}^{22} & c_{ij}^{23} \\ c_{ij}^{31} & c_{ij}^{32} & c_{ij}^{33} \end{bmatrix},$$

$$[k]=m_cV^2\begin{bmatrix} k_{ij}^{11} & k_{ij}^{12} & k_{ij}^{13} \\ k_{ij}^{21} & k_{ij}^{22} & k_{ij}^{23} \\ k_{ij}^{31} & k_{ij}^{32} & k_{ij}^{33} \end{bmatrix},$$

$$\{F\}=m_cg\begin{Bmatrix} F_i^1 \\ F_i^2 \\ F_i^3 \end{Bmatrix}, \quad \text{(B.1-5)}$$

where

$$m_{ij}^{11}=\phi_i^{(1)}\phi_j^{(1)},\ m_{ij}^{12}=-\mu\phi_i^{(1)}\phi_j^{(2)},\ m_{ij}^{13}=-\frac{h}{2}\phi_i^{(1)}\phi_j^{(3)},$$
$$m_{ij}^{21}=0,\ m_{ij}^{22}=\phi_i^{(2)}\phi_j^{(2)},\ m_{ij}^{23}=0,\ m_{ij}^{31}=\frac{h}{2}\phi_i^{(3)}\phi_j^{(1)},$$
$$m_{ij}^{32}=-\mu\frac{h}{2}\phi_i^{(3)}\phi_j^{(2)},\ m_{ij}^{33}=-\frac{h^2}{4}\phi_i^{(3)}\phi_j^{(3)},$$

$$c_{ij}^{11}=0,\ c_{ij}^{12}=-\mu\phi_i^{(1)}\phi_j'^{(2)},\ c_{ij}^{13}=0,$$
$$c_{ij}^{21}=0,\ c_{ij}^{22}=\phi_i^{(2)}\phi_j'^{(2)},\ c_{ij}^{23}=0,$$
$$c_{ij}^{31}=0,\ c_{ij}^{32}=-\frac{h}{2}\mu\phi_i^{(3)}\phi_j'^{(2)},\ c_{ij}^{33}=0,$$

$$k_{ij}^{11}=0,\ k_{ij}^{12}=-\mu\phi_i^{(1)}\phi_j''^{(2)},\ k_{ij}^{13}=0,$$
$$k_{ij}^{21}=0,\ k_{ij}^{22}=\phi_i^{(2)}\phi_j''^{(2)},\ k_{ij}^{23}=0,$$
$$k_{ij}^{31}=0,\ k_{ij}^{32}=-\frac{h}{2}\mu\phi_i^{(3)}\phi_j''^{(2)},\ k_{ij}^{33}=0,$$

$$F_i^1=-\phi_i^{(1)}\left(\mu\cos\theta+\sin\theta\right),\ F_i^2=\phi_i^{(2)}\cos\theta,$$

$$F_i^3=-\phi_i^{(3)}\frac{h}{2}\left(\mu\cos\theta+\sin\theta\right). \quad \text{(B.6-35)}$$

At any instant of time, ϕ_i, ϕ_i' and ϕ_i'' $(i=1,\ldots,7)$ must be calculated for $\varsigma=\varsigma_c$ and substituted into Eqs. (B.6)-(B.35), according to Eq. (13(b)).